

Complex study of the bioaerosol composition of the atmosphere over urban areas based on lidar monitoring during the quarantine COVID-19

Angelova B.², Iliev M.², Ilieva R.², Grigorov I.¹, Kolarov G.¹, Paneva D.³, Kolev Ch.³, Z. Cherkezova-Zheleva³, Groudeva V.², Stoyanov D.¹, Prof. Nedkov I.¹

¹ - Institute of Electronics, Bulgarian Academy of Sciences, Sofia, Bulgaria

² - Faculty of Biology, Sofia University "St. Kl. Ohridski", Bulgaria

³ - Institute of Catalysis, Bulgarian Academy of Sciences, Sofia, Bulgaria

E-mail for correspondence: nedkovivan@yahoo.co.uk

Abstract: A comprehensive study of the air condition in urban areas was conducted, based on lidar monitoring. The subject of monitoring are two districts of Sofia the capital of the R. Bulgaria. The time period of the study is May-June 2020 and coincides with the introduced quarantine period in connection with the COVID-19 pandemic. The study includes lidar monitoring of the selected urban areas taking into account the mass concentration of particulate matter (PM). The method is combined with in situ sampling taking into account also the size control in μm – PM_{2.5} and PM₁₀. The data are compared with those from the indications for the period of the licensed laboratories of the Ministry of Environment and Water and the Civil Network. A physicochemical study of the phase composition, structure and dispersion of the collected PM was performed by the methods of powder X-ray diffraction and Mössbauer spectroscopy. Predominant pollen and spore contamination was reported using Cascade Impactor measurements. Most part, the PMs studied show a conglomerate of several particles.

Keywords: BIOAEROSOL, PARTICULATE MATTER (PM), LIDAR MONITORING, PM SAMPLING

1. Introduction

Atmospheric pollution is a huge problem for the people living in big cities and is relevant through such planetary problems as global warming and damage to the ozone layer. Air pollution and urban air quality are listed as two of the world's worst toxic pollution problems in the 2013 and interest in it has been growing so far [1, 2, 3]. The present-day scientific interest over following the advances in measurement technologies [4. 5. 6. 7. 8. 9. 10.], which have allowed for monitoring the processes in the atmosphere and understanding of the biogenic composition and of the physicochemical properties of atmospheric particles. Particulate matter (PM) emitted by vehicles in urban traffic, seasonal heating and industrial activities, can greatly affect environment air quality and have direct implications on human health. This paper talks over the most recent results of air quality investigation at some residential districts of Sofia-the capital of R. Bulgaria within the application of Lidar monitoring of scanning the horizontal aerosol distributions and the vertical long-distance transport of air masses at operational distances exceeding 25 km. The studies were expanded with local sampling based on spatio-temporal data from lidar monitoring and indepth study of the bio-chemical and physical properties of PM. These studies are a natural continuation of our work covered in the book "Atmospheric Air Pollution Monitoring" [11].

2. Methods, instruments, and procedures

The lidar mapping was performed by a lidar system installed on the Lidar station of Institute of Electronics. The site at residential district Mladost is located at a distance about 3 km and Dragan Tsankov blvd. is at a distance of 5.5 km from the lidar. This lidar system is capable of scanning the horizontal and vertical aerosol distributions and transport of air masses with a spatial resolution of 30 m and a beam divergence of ~ 1 mrad at operational distances of about 25 km. The laser emitter (wavelength of 510.6 nm) is a pulsed CuBr vapor laser with a repetition rate of 10 KHz at a 15-ns pulse duration. The receiving system comprises a Carl Zeiss Jena Cassegrain telescope (aperture of 20 cm, a focal distance of 1 m), a 2-mm-wide focal diaphragm, an interference filter with 2-nm-wide passband, and an EMI 9789 photo-multiplier tube operating in a photon-counting mode. The receiving system is fully computerized for collecting and processing the lidar data using a PCO 1001 1024-channel digital interface system for signal strobing and accumulation.

The PM sampling were realized using Andersen Cascade Impactor [12]. For enumeration of microbiota into the atmospheric

air, an active sampling with FSC-A6 1CFM impactor was engaged. Glass Petri dish (ϕ 90x15 mm) with 27 ml sterile nutrient media was positioned beneath each stage. Nutrient agar with cycloheximide was used for bacteria and YGC agar for fungal enumeration. The Petri dishes were incubated for 48h at room temperature (25°C). The positive hole method and expressed as CFU/m³ was used for total colony counts (Andersen, A.A, 1958). The control and selection of particles by size and mass concentration in this experiment was expanded through systematic use during lidar experiments and in the daily experimental practice of the Microcontroller SDS 011 – PM_{2.5} и PM₁₀. Additionally, the material collected on the filters and the stage after three hours of aspiration during the lidar monitoring was studied by SEM and EDAX. Mössbauer analysis was made using a Wissenschaftliche Elektronik GmbH apparatus, working at a constant acceleration mode; ⁵⁷Co/Cr source, α -Fe standard. The parameters of hyperfine interactions of the Mössbauer spectral components were determined by computer fitting.

3. Results and discussion

The city of Sofia has a well-developed control network of local licensed stations for daily pollution control in selected points of the town. The subject of this study is to compare the network information with the lidar measuring during the months May and June 2020, which are part of the quarantine period of the COVID-19 pandemic. The measurement of pollution for the period shows a relatively low concentration of PM, which is due to understandable reasons of limited traffic and relatively warm weather for the season (average monthly temperature in the range of 16-20°C), which significantly reduces the use of heating appliances, respectively the use of solid fuels. The limited traffic opens a good opportunity to study the contribution of organic particles and especially those related to the flowering of plants, which is typical for the second haft of May and the beginning of June. In the second haft of June, significant relief was introduced in quarantine measures and industrial life returned to its traditional activities. Although the pollution did not exceed the critical values [13], we conducted in-depth studies of the PM and microbial contents (Mladost and Lozenets), where more than 160 thousand citizens live.

3.1. Lidar monitoring

Analyzing the PM in aerosol loadings formed in the vicinity of the grounded level of the atmospheric urban areas and experimentally measured of the mass concentration of the aerosol by the lidar technique were able to draw the important conclusion. Two major lidar parameters were calibrated, namely, the extinction

coefficient $\alpha(r)$ and the backscatter coefficient $\beta(r)$, in terms of the aerosol mass concentration following the well-known method [10,13] and making use of the mass concentration M_a data obtained by the sampling device. For the lidar ratio $LiR = \alpha(r)/\beta(r)$ we adopted the typical value of $LiR = 50$ [10,13]. The parameters $\beta(r)$ and $\alpha(r)$ were calculated using the lidar equation under the assumption of a horizontally-homogeneous atmosphere:

$$P(r) = P_0 \frac{c\tau}{2} C \frac{\beta(r)}{r^2} \exp\left[-2 \int_{r_0}^r \alpha(r) dr\right] \quad (1)$$

where $P(r)$ is the power of the detected laser radiation backscattered from the atmosphere from a distance $r = \frac{ct}{2}$ after a period of time t following the moment of laser pulse emission, and τ is the pulse duration. Under the homogeneity assumption, the extinction coefficient $\alpha(r)$ is calculated as

$$\alpha(r) = -\frac{1}{2} \frac{dS(r)}{dr}, \text{ where } S(r) = \ln[r^2 P(r)] \quad (2)$$

Calibration dependencies of the mass concentration in [mg/m^3] of, respectively, $\alpha(r)$ and $\beta(r)$ was developed. In both cases, the linear fit ($Y=A+B.x$) shows acceptable values of the standard deviation (less than 4 %) and the correlation coefficient (over 0.92). The plots can be used directly for calibrating the lidar maps, shown above, in mass concentration.

The lidar observation schedule complied with the generally accepted manner of measuring the aerosols mass concentration by air-quality monitoring systems. The sampling device pumps atmospheric air through the filter (typically a volume of 60–100 m^3) for an interval of about a few hours. Thus, the laser beam was stationary and directed to pass above the aspirator at a height of $h_{PM} < \delta R$, $\delta R \sim 30m$ being the lidar's radial resolution. The height of placing the aspirator was also chosen to comply with this condition, $h_{asp} < \delta R$. The lidar signals represent the number of backscattered photons $L_{phot}(k.\delta R, \tau_m)$, where $k=1..K_{max}$, $K_{max} = R_{max}/\delta R$, and $\tau_m = 5 \text{ min}$ is the time of photons accumulation. The total time of measurement lasted from one to several hours, depending on the particular weather situation. The computer system processes the input data by solving the lidar equation (1), with its output being profiles of the backscatter coefficient $\beta(k.\delta R)$ or the extinction coefficient $\varepsilon(k.\delta R)$, as calibrated in terms of aerosols mass concentration (see Fig. 3 above). The set of lidar profiles obtained for the entire period of measurement is used to construct 3D lidar maps, with the x axis presenting the accumulation time with a step of $\tau_m = 5 \text{ min}$ and the y axis, the distance from the lidar with a step δR . The z axis corresponds to the color-coded coefficients of backscatter or extinction.

The lidar monitoring of the selected areas was carried out with a starting point – Lidar station of the Institute of Electronics, as the laser beam is horizontal at a height of about 40 m and its direction is marked on the city map (see Fig.1). The lidar measurements were also performed with inclined lidar drilling with a variable angle to the horizon, as the height at the end of the route reaches a height of 2 km. Fig.1b shows a lidar map in the form of a corner sector of daily observation (19.05.2020), which well illustrates the capabilities of the lidar and is a typical lidar image for the studied period. Fig.1a for comparison shows the lidar map of a typical image for April 2019.

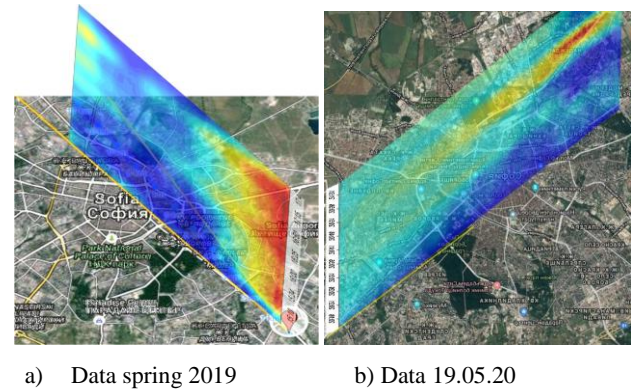


Fig. 1 a) Lidar sector mapping of pollution measured in April 2019 and b) measured in May 2020 (graduation from light blue to dark brown shows an increase in the mass concentration of PM)

Figures 1a and 1b well illustrate the difference between the pollution found by the lidar during the quarantine period and the conventional state of the atmospheric pollution in the same caisson but with heavy traffic. Apparently in the COVID-19 quarantine period the surface atmospheric layer has a very low concentration of PM. The data from the lidar monitoring shown in Fig.1 make it possible to obtain fast and accurate information in time-space coordinates. It is evident that for the studied period the pollution in the ground layer of the urban atmosphere is insignificant, but the lidar makes it possible to report pollution in the higher layers of the atmosphere.

The dependence of the aerosol extinction coefficient in the surface atmosphere on the distance to the Lidar station was also investigated. This coefficient is one of the most accurately measured optical parameters of the atmosphere and is used to calibrate lidar signals at mass concentration [11]. The data shows that the surface aerosol atmosphere is almost homogeneous at distances up to over 8 km from the location of the lidar and varies in small ranges from 0.01 to about 0.03 micrograms per cubic meter. At these extinction values, the atmosphere can be considered clean during the quarantine period, which is mainly due to the greatly reduced car traffic, as well as the reduced industrial activity of the citizens due to the state of emergency. It can be expected that by May and the beginning of June 2020 the air quality has improved.

3.2. Particle size distribution studies

In order to better assess the accuracy of lidar monitoring, in parallel with daily pollution measurements were made using electronic sensors type Microcontroller SDS 011, which detects pollution with PM2.5 and PM10. The controllers were located at a height of 10 m from the ground. Our measurements were compared with data from licensed stations and those of the civil network.

Below in Fig.2 shows histograms that illustrate well the approach to these measurements. Data from 05 and 06 May 2020 were selected, in which relatively high pollution was reported. This is a time when the merger of two weekends ends and during which there was an increase in car traffic of vacationers returning to the capital. Our measurements are compared with the data from the nearest measuring points of the licensed network of the Ministry of Environment and Water and of the civil network of the Cleanliness Movement. The results were obtained using an electronic tester type Microcontroller SDS 011 for PM2.5 and PM10. The survey was conducted daily in May and June 2020. Fig.2 illustrate the approach in measuring pollution.

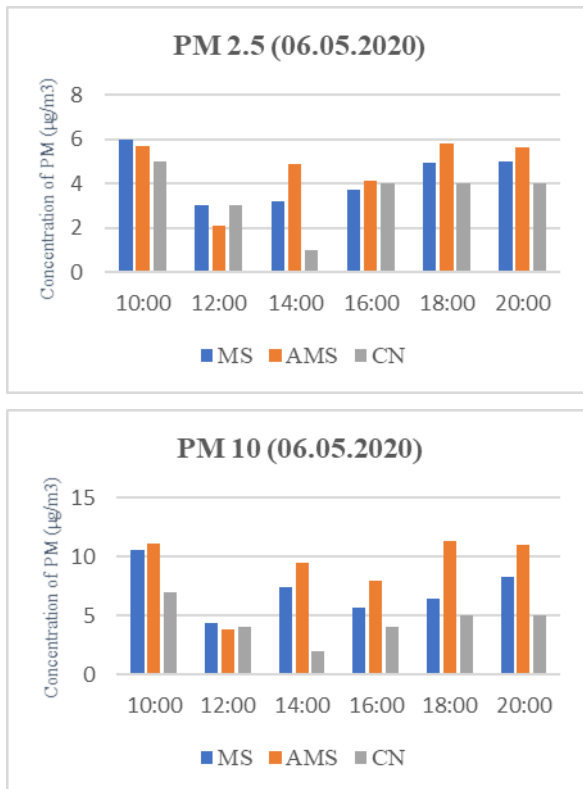


Fig. 2 Data about the PM_{2.5} and PM₁₀ for three points of the district Mladost (MS – mobile sensor data, Mladost 1; AMS – licensed air monitoring station data, Mladost 1; CN – civil network data, Mladost 2).

In our measurements, the influence of the parameters – temperature, humidity, wind speed and atmospheric pressure – was taken into account in parallel. The data are shown in Table 1.

Table 1: Meteorological data during the measurement

	T (°C)	Relative humidity (%)	Wind (m/s)	Atmospheric pressure (hPa)
10:00	7	80	3.1	1014
12:00	9	82	3.1	1014
14:00	9	82	3.6	1015
16:00	8	87	5.7	1015
18:00	7	80	2.0	1016
20:00	9	71	5.1	1014

From the above data it can be seen that in practice we have two maximums of pollution – in the morning until 10.00 h and after 18.00 h. These peaks are repeated systematically on a monthly basis. In practice, the measurements of pollution with controllers coincide well with the lidar data for relatively high air purity (low mass concentration of PM) and similarity of pollution in large urban areas. This finding gave us reason to unify the measurements with those of the licensed stations near which our results were compared. For this purpose, a method for calibration was developed.

3.3. Calibration of sensor data

Below we will describe the algorithm applied for calibration of sensor data. The measured data are presented as time series, denoted by:

$$X(t_k), t_k = t_0 + \Delta k, k=1..N \quad (3)$$

where Δ is the sampling interval, t_k are the successive sampling instances, N is the total number of single measurements and $T_m = N \cdot \Delta$ is the full measurement time. Moreover, the variables $X(t_k)$ present the sensor measured separately PM_{2.5} & PM₁₀ mass concentrations in ($\mu\text{g}/\text{m}^3$).

Following the expression in (3) the reference data can be presented as well by

$$Y(t_k), t_k = t_0 + \Delta k, k=1..N \quad (4)$$

They are collected simultaneously by the officially calibrated Station (IOS) of the Sofia Municipality, disposed nearby to about 70m. The reference sensor data are given as well separately for the both particle types PM_{2.5} & PM₁₀ respectively.

In the further analysis we will accept the aerosol filed, carrying the aerosol PM_{2.5} & PM₁₀ particles in the region of measurements as approximately uniform and stationary during the measurement time T_m . Then, we could calculate separately from (3, 4) the total mass concentrations for the both types PM_{2.5} and PM₁₀, given by :

$$MX^{\text{PM}_{2.5}} = \sum X^{\text{PM}_{2.5}}(t_k), k=1..N; MX^{\text{PM}_{10}} = \sum X^{\text{PM}_{10}}(t_k), k=1..N; \quad (5)$$

$$MY^{\text{PM}_{2.5}} = \sum Y^{\text{PM}_{2.5}}(t_k), k=1..N; MY^{\text{PM}_{10}} = \sum Y^{\text{PM}_{10}}(t_k), k=1..N; \quad (6)$$

where $MX^{\text{PM}_{2.5}}, MX^{\text{PM}_{10}}$ in (4) are the sensor's measured total mass concentrations and $MY^{\text{PM}_{2.5}}, MY^{\text{PM}_{10}}$ in (5) are the corresponding total mass concentrations, measured by the Municipality reference Station. As seen in (4) and (5) the calculated total mass concentrations are averaged quantities over the entire measurement time T_m at the assumption for the uniform and stationary aerosol field.

One can now calculate the calibration coefficients to the sensor time series in (3) using the ratios R_0^{PM} for both particle types PM_{2.5} & PM₁₀ respectively, using (4), (5) and given by:

$$R_0^{\text{PM}_{2.5}} = MY^{\text{PM}_{2.5}} / MX^{\text{PM}_{2.5}}; R_0^{\text{PM}_{10}} = MY^{\text{PM}_{10}} / MX^{\text{PM}_{10}} \quad (6a)$$

At least, using the expressions in (6) the calibrated quantities $X_{\text{cal}}(t_k)$ in the sensor measured PM mass concentrations $X(t_k)$ can be presented by

$$X_{\text{cal}}^{\text{PM}}(t_k) = R_0^{\text{PM}} \cdot X^{\text{PM}}(t_k), t_k = t_0 + \Delta k, k=1..N, \quad (6b)$$

The effects of the calibration algorithm above developed on the time history of the measured time series $X^{\text{PM}_{2.5}}(t_k)$ and $X^{\text{PM}_{10}}(t_k)$ by the both types of sensors: of IE-BAS and the Civil network are presented on Fig.3a to 3e below. Here the plot in Fig.3a presents ratio of both mass concentrations of PM_{2.5}/PM₁₀, measured by the Reference station used also for the calibration of other two groups of sensors. As seen, the ratio PM_{2.5}/PM₁₀, averaged over the entire period from March 7 to March 25 is of order of 0.48-05, which is typical for the clear atmosphere conditions. Moreover, the time-variations of the same ratio PM_{2.5}/PM₁₀, displayed as time series are given in Fig.3b. As seen, some non-strong air pollution are detected during the first half of the measurement period, when the same ratio is of order of 0.5, remaining relatively constant on the 0.5 level up to the end of the measurement period.

The effects of the calibration algorithm are further demonstrated on the next Fig. 3c3 to 3c5. Here the ration PM_{2.5}/PM₁₀ is calculated from the non-calibrated data, acquired by the sensors in the civil network. As seen in Fig.3c3, here the PM_{2.5}/PM₁₀ varies within the limits of 0.4 to 0.6 for the first period as in Fig. 3c2. Then, during the last quarantine period the same ratio is rapidly increased up to the values of 1.6. As seen in Fig.3b such of high increase of the ratio PM_{2.5}/PM₁₀ was not observed in the previous Fig.3b. The next Fig.3c demonstrates the time history of the same ratio PM_{2.5}/PM₁₀ calculated from the same data as in previous figure, but after their calibration, according to the above Calibration algorithm. As seen, the variations of the same ratio within the first period remains within the same limits as in the first two figures. Moreover, the step increase of the ratio PM_{2.5}/PM₁₀ on the final quarantine period is missing here. This result is very important as it demonstrate the effectiveness of the Moreover, the same behavior of the ratio PM_{2.5}/PM₁₀ is displayed on the last Fig.3e, where the calibrated data from the IE sensors are shown. We will note that the mean ratios, calculated from calibrated data remains very close as shown in all of figures. As a conclusion, it could be stated, the calibration algorithm here developed could be useful in many cases

for calibration of sensors over large networks, using a single reference station.

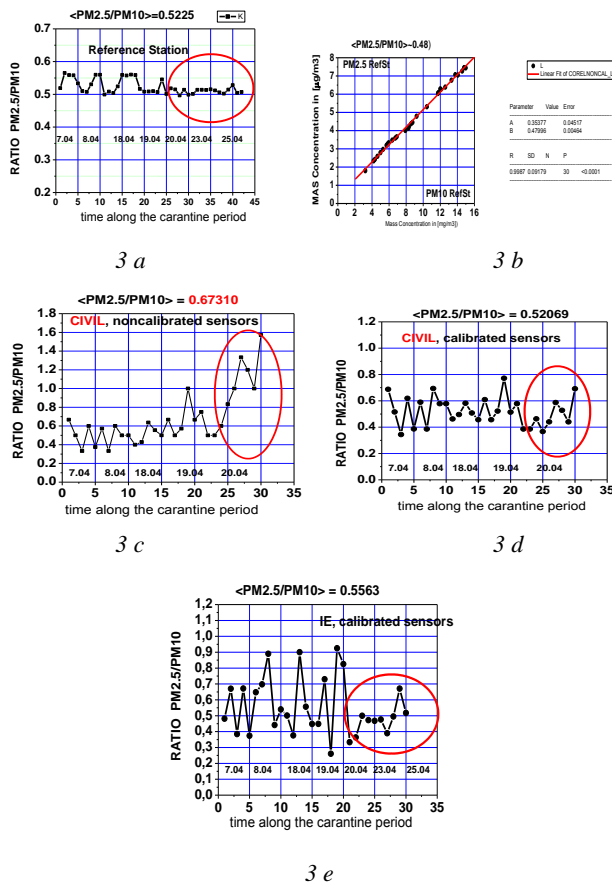


Fig. 3 Summarized calibrated data from our measurements for May and June 2020 for PM2.5 and PM10 pollution (Sofia's districts Mladost and Lozenets)

3.4. Crystallochemical features of PM

The recorded X-ray diffractograms show that the examined PMs are X-ray amorphous. No crystalline phases were detected. One of the diffractograms is presented on Fig.4 and well illustrate the structural features of the PM.

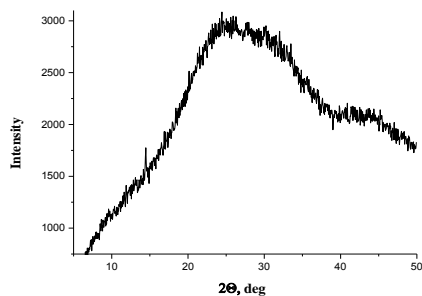


Fig. 4 X-ray diffraction pattern of PM, which illustrates their amorphousness and absence of crystalline phases.

Mössbauer's analyzes of the studied PMs show the presence of iron ions in the second valence of oxidation, mostly in the atmosphere of district Lozenets, while equal amounts of divalent and trivalent iron were registered in the samples from district Mladost. The absence of sextet (magnetic) components and the presence of a predominant amount or entirely divalent iron is characteristic of PM with natural origin – mineral or biologic. Which can explain the amorphous structure illustrated in fig.4.

3.5. Quantitative characteristics of the microbial component in the selected locations

Quantitative analysis was performed to determine the total number of cultured microorganisms as follows: aerobic heterotrophic bacteria (NA medium) and fungi (YGC medium). Samples were collected twice for each month (1 and 4 weeks) by means of a six-stage cascade impactor and performed in triplicate for each sample.

The results of the analysis show a significantly higher number of bacteria compared to that of fungi in both time intervals of the study. When comparing the data from this analysis over time: May, 2020 and June, 2020, a significant increase in the number of the two studied groups is reported. As already mentioned, the first interval tested in May is characterized by extremely low anthropogenic pressure due to the quarantine sanitary-epidemiological restrictions for the period (Fig. 5).

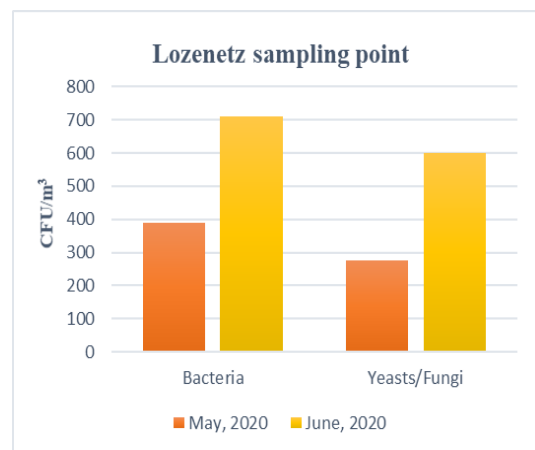


Fig. 5 Quantitative characteristics of the microbiota in Lozenets location

Cascade impactor aspiration methods are currently considered to be one of the most suitable for quantifying the microbial component, as they provide information on the size distribution of bioaerosol particles. The distribution of bioaerosols, respectively their precipitation and stability depend to a large extent on the size of the bioaerosol particles. The data from the comparative analysis of bacteria and fungi depending on the size of the bioaerosol particles in the above location are given in Table 2.

Table 2: Quantitative characteristics of bacteria and fungi depending on the size of bioaerosol particles in Lozenets location

Size of bioaerosol particles (µm)	Location Lozenets			
	Bacteria (CFU/m ³)		Fungi (CFU/m ³)	
	May	June	May	June
I – 0.65 – 1.1	3.1±0.2	8.5±0.3	0	0
II – 1.1 – 2.2	13.2 ±0.1	39.5±0.2	8.1±0.1	91.3±0.3
III -2.1 – 3.3	75.8±0.5	125.2±0.1	45.2±0.1	161.1±0.1
IV – 3.3 – 4.7	99.6±0.4	160.4±0.1	95.2±0.1	205.3±0.1
V – 4.7 – 7.0	90.3±0.1	171.8±0.2	37.5±0.1	78.2±0.1
VI - > 7.0	110.5±0.3	207.2±0.3	90.2±0.2	42.5±0.2

The results obtained show domination of bacterial bioaerosol particles with sizes over 7.0 µm, followed by those with sizes 4.7 - 7.0 µm; 3.3 - 4.7 µm and 2.1 - 3.3 µm. The cascade impactor does not allow the ingress of a particle larger or smaller than the corresponding level of the pores. This proves that the association of microbial cells with PM, leading to the formation of an aggregate of a certain size. The analysis of the size distribution of the fungal bioaerosol particles reveals the highest share of particles with sizes 2.1 - 3.3 µm and 3.3 - 4.7 µm.

4. Conclusions

In general, the following main conclusions are outlined: 1. Quarantine period has led to a sharp reduction in PM pollution. Traffic and the use of solid fuel for heating are strongly reduced and this is underlined by the data on lidar monitoring for the same period in 2019 and the increase in pollution while easing the quarantine measures (after 13.06.20). 2. The greatly reduced presence of PM due to traffic and heating has opened up a good opportunity to take into account the presence of microbial contamination in the ground layers of the atmosphere. 3. Their presence is either as well-formed microbially contaminated PMs in the form of bioaerosols associated with inorganic PMs. 4. The amount of microbiota (bacteria and fungi) increases significantly after the relief of the quarantine period, which shows a direct relationship between the inorganic and microbial content of PM.

5. Acknowledgments

This work was financed in part by contract DN18/26 with the National Science Fund, Bulgaria, and included in the European Program of the COST Action CA16202.

6. References

1. Blacksmith Institute (New York). The World's Worst 2013: The top ten toxic threats - Cleanup, Progress, and Ongoing Challenges. (2013).
2. P.Thunis, B. Degraeuwe, E. Pison, M. Trobrtti, E. Peduzzi, C.A. Belis, J. Wilson, E. Vignati, Urban PM2.5 Atlas Air quality in European cities, Ed. By JRC and European Commission, (2017).
3. Environmental monitoring of bioaerosols at regulated facilities, Environment Agency, July 2018
4. G. Fernald. Analysis of atmospheric lidar observations: some comments. *Applied Optics*, **23**(5):652 (1984).
5. T. Song, Z. Liu, T. Hu. Application of Atmospheric Particles Monitoring based on MODIS Aerosol Optical Thickness Products and Laser Radar. *Remote Sensing Technology and Application*, **31** (2):397-404 (2016).
6. B. Zu. Research on Application of Multiple Particle Lidar for Environmental Monitoring. *Journal of Green Science and Technology*, **10**:122-124, (2018).
7. D. Xu, Q. Zhang, Q. Fan. Study on Characteristics of Particulate Matter Pollution in Hangzhou and Surrounding Areas Based on Lidar Observation Network. *Journal of Atmospheric and Environmental Optics*, **14**(03):171-178, (2019).
8. W. H. Zhao, L. Yan, C. Y. Wang. Detection of Atmospheric Particulate Matter Pollution Based on Three -Dimensional Atmospheric Detection Lidar. *Geomatics and Information Science of Wuhan University*, **44**(10):1436-1441 (2019).
9. R. J. Allen, W. E. Evans. Laser radar (LIDAR) for mapping aerosol structure *Review of Scientific Instruments* **43**, 1422 (1972).
10. F. Fernald, Analysis of atmospheric lidar observations: some comments, *Appl.Opt.* **23**, (5), pp.852-853 (1984)
11. Stoyanov D., I. Nedkov, V. Grudeva, Z. Cherkezova-Zheleva, I. Grigorov, G. Kolarov, M. Iliev, R. Ilieva, D. Paneva, C. Ghelev. Long-Distance LIDAR Mapping Schematic for Fast Monitoring of Bioaerosol Pollution over Large City Areas. *Atmospheric Air Pollution and Monitoring*. Ed. A. Lakhout, ISBN: 978-1-78985-280-6, Publ. IntechOpen, London (2019)
12. M. King, A. R. McFarland. Use of an Andersen Bioaerosol Sampler to Simultaneously Provide Culturable Particle and Culturable Organism Size Distributions, *Aerosol Science and Technology*, **46**:8, 852-861, (2012).
13. Air Quality Directive and the guidelines for fine particulate matter PM2.5 and PM10 recommended by the World Health Organization (2017).
<https://www.euro.who.int/en/health-topics/environment-and-health/air-quality/publications/2017/evolution-of-who-air-quality-guidelines-past,-present-and-future-2017>
14. J. Klett. Stable analytical inversion solution for processing lidar returns, *Appl.Opt.* **22**, pp.211-220 (1981).
15. A. Andersen. New sampler for the collection, sizing, and enumeration of viable airborne particles *J. Bacteriol.*, **76**, 471-481, (1958).
16. J. D. Wilcox. Design of a new five-stage cascade impactor. *AMA Arch Ind Hyg Occup Med.* **7**(5), 376-382, (1953).